Oxidative Esterification of 5-Hydroxymethylfurfural under Flow Conditions Using a Bimetallic Co/Ru Catalyst

Abel Salazar,[a] Alexander Linke,[a] Reinhard Eckelt,[a] Antje Quade,[b] Udo Kragl,[c, d] and Esteban Mejía*[a]

Furanic di-carboxylate derivatives of 5-Hydroxymethylfurfural (HMF) are nowadays important in the polymer industry as they are used as building blocks for bio-based polyesters. The high reactivity of HMF compels to avoid harsh synthetic conditions. Therefore, developing mild catalytic processes for its selective oxidation is a challenging task. Herein, we report the first oxidative esterification of HMF to dimethyl furan-2,5-dicarboxylate (FDCM) under flow conditions using oxygen as oxidant. For that purpose, a new series of nitrogen-doped carbon-supported bimetallic Co/Ru heterogeneous catalysts were prepared and characterized by XRD, XPS and N_2 physisorption. These analyses revealed that the porosity of the materials and order of impregnation of the metals to the carbon supports lead to varying catalytic activities. Under optimized conditions the flow reactor showed a 15-fold increase on the production of FDCM compared to batch conditions.

Introduction

Nowadays, obtaining platform chemicals from renewable sources is a highly relevant topic due to the necessity to reduce society's dependence in oil-derived resources. The use of biomass-derived platform chemicals is a step forward in achieving a sustainable circular economy,[1] bringing molecules like 5-hydroxymethylfurfural (HMF, **1**) to the spotlight.[2] HMF is the basis of furanic polymers,[3] where polyethylene furanoate (PEF) stands as a promising substitute of polyethylene terephthalate (PET), as it can be produced entirely from renewable sources.[4]

The biomass-based production of PEF (Scheme 1) commonly starts with acidic or enzymatic hydrolysis of cellulose to obtain C_6-sugars (e.g. glucose, fructose) from which dimethyl-2,5-furandicarboxylate (FDCM, **2**) and ethylenglycol (EG) can be synthesized. HMF is obtained by the dehydration of sugars (preferably fructose);[5] FDCM can be obtained from the oxidative esterification of HMF in MeOH, while EtOH is obtained from the fermentation of sugars,[6] and dehydrated to produce ethylene.[7] The latter can be converted into EG by various established industrial oxidation methods. Finally, PEF is synthesized by a 2-stage step-growth polymerization between FDCM and EG.[8]

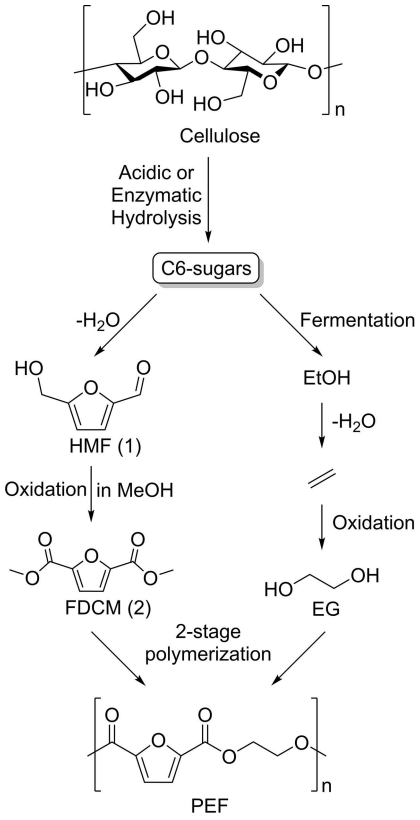

Scheme 1. Production of polyethylene furanoate (PEF) from biomass.

[a] *A. Salazar, A. Linke, R. Eckelt, Dr. E. Mejía*
Leibniz-Institute für Katalyse e. V.
Albert-Einstein-Straße 29A
18059 Rostock (Germany)
E-mail: esteban.mejia@catalysis.de
[b] *Dr. A. Quade*
Leibniz-Institut für Plasmaforschung und Technologie e. V.
Felix-Hausdorff-Str. 2
17489 Greifswald (Germany)
[c] *Prof. U. Kragl*
Institut für Chemie, Technische Chemie
Universität Rostock
Albert-Einstein-Straße 3A
18059 Rostock (Germany)
[d] *Prof. U. Kragl*
Department Life, Light and Matter
Universität Rostock
18051 Rostock (Germany)

Supporting information for this article is available on the WWW under https://doi.org/10.1002/cctc.202000205

In order to make PEF economically viable, the production of FDCM or its analogs (e.g. 2,5-furandicarboxilic acid, FDCA) must be improved, either by catalyst development or by using new synthetic methods. FDCM is a more promising monomer than FDCA since it is easier to purify, is more stable under polymerization conditions and shows increased reaction rates.[8] Taking this into consideration, we focused our efforts towards the synthesis of FDCM from HMF.

The use of oxygen gas as terminal oxidant in organic synthesis is an attractive goal as it is readily available and non-toxic.[9] Nevertheless, its usage has had limited spread due to safety concerns and the poor solubility of O_2 in most solvents.[10]

Microflow technologies are gaining increasing popularity in organic synthesis due to its improved safety, and the possibility to precisely control mass-transport and processing parameters. Hence, microflow reactors represent a safe alternative to batch systems since the smaller reactor volumes minimize the severity of an accident. At the same time, the accumulation of hazardous/unstable intermediaries is minimized. Moreover, the possibility to accurately dose gaseous reactants and the lack of a headspace (virtually unavoidable under batch conditions) reduce significantly the risks of accidents.[11] As a consequence of the reduced size components, different physical parameters can be optimized to a higher level under microflow conditions, compared to the standard laboratory and industrial batch conditions (e.g. mass and heat transfer, mixing, etc.).[12] More importantly, mass transfer limitations are reduced to the minimum,[13] which helps to circumvent the restrictions of working with low solubility gases like oxygen.[14] Last, but not least, the development of processes under microflow conditions allows the possibility of a scale-up with relative ease.[15]

Herein we report the development and characterization of carbon-supported bimetallic cobalt/ruthenium catalysts and their application in the first oxidative esterification of HMF under flow conditions, to produce FDCM with very high conversion and good selectivity.

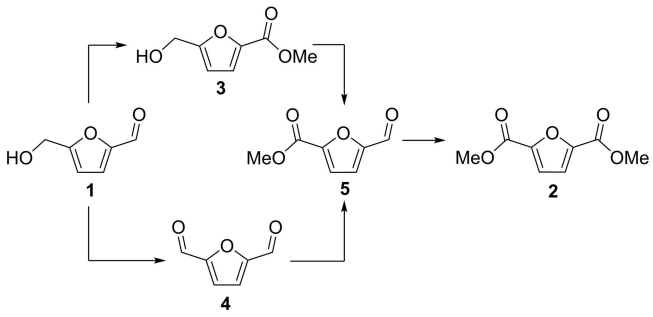

Scheme 2. Divergent reaction pathways for the oxidative esterification of HMF (**1**) to produce FDCM (**2**).

Results and Discussion

As shown in Scheme 2, the oxidative esterification of HMF (**1**) to produce FDCM (**2**) can be achieved in a divergent, multistep process. HMF is first converted either to methyl 5-(hydroxymethyl)furan-2-carboxylate (**3**) or to furan-2,5-dicarbaldehyde (**4**). Both 3 and 4 can be converted to methyl 5-formylfuran-2-dicarboxylate (**5**). Finally, aldehyde oxidative esterification leads to the desired product (**2**). Both conversion and selectivity depend on the catalyst used and its activity, as previously demonstrated in the oxidation of HMF to FDCA.[16]

In a previous work, we reported the aerobic oxidative esterification of **1** to **2** using a mixture of carbon-supported nitrogen-doped cobalt and commercial ruthenium catalysts (Co_xO_y–N@C and Ru@C) in a batch reactor.[17] In order to incorporate both metals in the same support, new powdered catalysts were prepared and explorative tests were done. The results were promising: $>99\%$ of HMF conversion was achieved with a selectivity of 38% of **2**, 47% of **3**, and 8% of **5** (see Supp. Info). With this in mind and knowing the limitations of batch reactors, we moved on to perform the reaction in a flow regime.

The reactor setup is presented in Scheme 3. It begins with having both gas and liquid phases separated. In the liquid part, a selector valve allows to choose the feed from either pure solvent or substrate solution. The two phases (gas and liquid) are then mixed before going into the reactor. The mixer is based on the multilamination principle, providing the ideal conditions for gas/liquid mixing.[13] The setup contains a pressure gauge as well as a temperature indicator. The reactor is heated with a fitted thermostat. Additionally, for safety control, a pressure release valve was used. At the reactor outlet the product mixture is cooled down in a water/ice bath, and sampled for analysis.

When powdered catalysts (analogous to those used in the aforementioned batch experiments) were used in the microflow reactor, technical problems arose. The fine catalyst particles packed in the cartridge led to a pressure increase in the system above the maximum input pressure of oxygen. As a consequence, oxygen could not be fed into the system anymore. In an attempt to avoid this problem, the powdered catalyst was "diluted" with glass beads and glass wool, alas, unsuccessfully. Layering of the catalyst with glass spheres lead to a slight improvement, although the catalyst particles were too small to be contained in the cartridge and small amounts of catalyst were collected along with the product at the system outlet. Increased temperatures shown to be detrimental as well since **1** decomposes above 150 °C.

Therefore, a new series of nitrogen-doped Co and Ru-based catalysts was synthesized using different types of carbon supports, and changing the order in which the metals and ligands are impregnated into them. We selected carbon particles of irregular shape ($-20+40$ mesh) and cylindrical pellets (~0,8 mm diameter), which will be called from now on *C-irregular* and *C-pellets*, respectively (See figure 1). This simple changes in the supports' morphology allowed us to operate the reactor under the desired conditions and prevent catalyst loss.

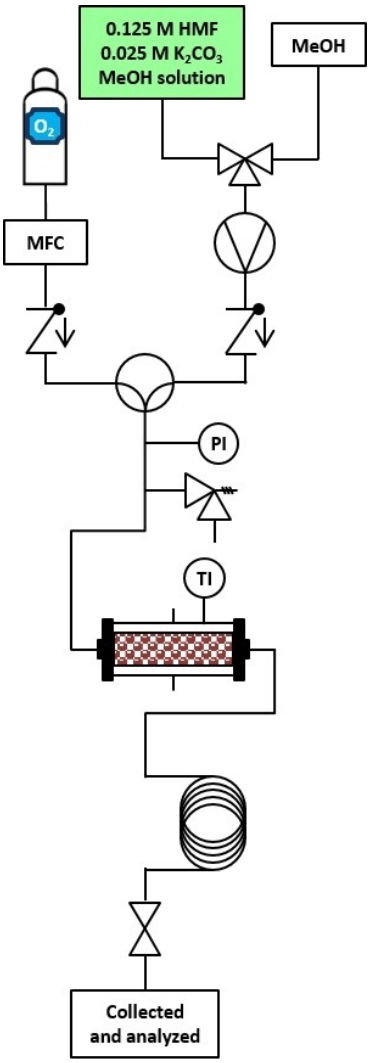

Scheme 3. Flow diagram of the microreactor setup used for the synthesis of FDCM (**2**) from HMF (**1**) under aerobic conditions.

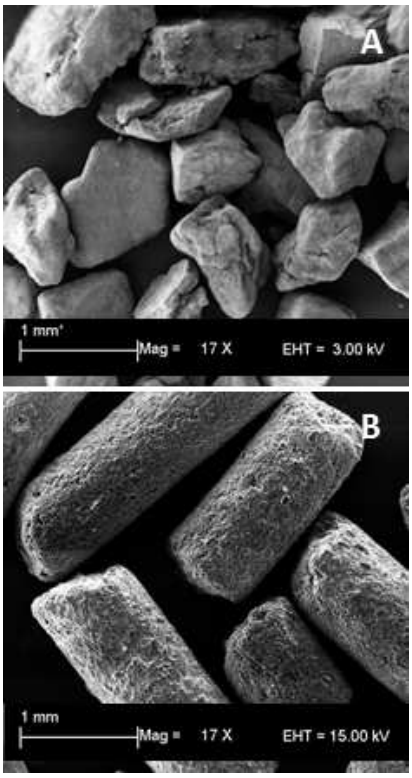

Figure 1. SEM images of the carbon supports used. (A) particles of irregular shape (−20 + 40 mesh, C-irregular) and (B) cylindrical pellets (~0,8 mm diameter, C-pellets).

Table 1. Catalyst screening for the oxidative esterification of HMF (1) under flow conditions.

Entry[a]	Catalyst	Conv. [%]	Product selectivity [%]				
			2	3	4	5	Others
1	Co_xO_y–N@C-pellets	57	4	72	12	-	12
2	RuO_x–N@C-pellets	60	4	–	66	25	5
3	Co_xO_y–N + RuO_x–N@C-pellets	44	5	46	20	–	29
4	RuO_x–N + Co_xO_y–N@C-pellets	66	15	52	11	–	22
5	Co_xO_y–N@C-irregular	92	18	63	4	–	15
6	RuO_x–N@C-irregular	35	3	-	54	11	31
7	Co_xO_y–N + RuO_x–N@C-irregular	98	57	20	1	1	21
8	RuO_x–N + Co_xO_y–N@C-irregular	73	27	45	8	–	20
9	Mixture entry 5 – entry 6	62	15	50	11	1	23

[a] Reaction conditions: 600 mg catalyst loading, 0.2 mL/min of a MeOH solution of 0.125 M HMF and 0.025 M K_2CO_3, 1,4 mL/min of oxygen, reactor temperature: 62 °C, autogenous pressure, residence time in reactor: 10 min.

The catalyst screening was focused on maximizing the conversion of **1** and the selectivity towards **2** above intermediates **3**, **4** and **5**. As presented in Table 1, when the cobalt-based catalysts were used (entries 1 and 5) selectivity (up to 73%) towards **3** was observed for both types of supports. The catalyst Co_xO_y–N@C-irregular (entry 5) showed an excellent conversion of **1** (92%) although only with poor selectivity towards **2** (18%). In comparison, Co_xO_y–N@C-pellets (entry 1) only showed a modest conversion (57%) and very poor selectivity (4%) towards **2**. In the case of the ruthenium-based catalysts, (entries 2 and 6), high selectivity towards **4** was observed. Contrary to the cobalt catalysts, conversion up to 60% was obtained with RuO_x–N@C-pellets (entry 2) and only 35% with RuO_x–N@C-irregular (entry 6). The latter also showed the highest amount of side products in the catalyst screening (up to 31%). For the cobalt catalysts, the best support seemed to be C-irregular and surprisingly, for the ruthenium, C-pellets. Up to this point, the reactivity and selectivity of the catalysts is similar to what was observed previously in the batch reactor.[17] It must be highlighted that the nitrogen doping has no detrimental effect on the catalytic activity of the ruthenium catalysts. While commercial Ru@C is commonly prepared by reduction in H_2 atmosphere,[18] our RuO_x–N@C catalyst was made by pyrolysis under argon atmosphere, analogous to Co_xO_y–N@C. This change in the preparation method simplifies the synthesis of

the catalysts, removing the difficulty of preparing a bimetallic catalyst with different oxidation states. Importantly, the morphology changes of the support didn't affect the catalytic activity.

When a mixture of Co_xO_y–N and RuO_x–N@C catalysts was used (entries 3 and 7), remarkable differences in conversion and selectivity were observed. Using C-pellets as support (entry 3) a conversion of only 44% was observed, with selectivity toward products **3** and **4** of 46% and 20% respectively. On other side, C-irregular (entry 7) as support gave the best results of the catalyst screening, where conversion up to 98% was achieved with a selectivity of 57% towards the desired product **2**. In addition, RuO_x–N + Co_xO_y–N@C catalysts (entries 4 and 8) show moderate to good conversions, 66% for C-pellets (entry 4) and 73% for C-Irregular (entry 8) with selectivity of 52% and 45% for **3** and 15% and 27% for **2** respectively. We also checked the catalytic performance of a physical mixture of Co_xO_y–N@C-irregular and RuO_x–N@C-irregular (entry 9). 62% conversion was obtained with selectivity of 50% and 15% towards **3** and **2** respectively. This result confirms that the presence of cobalt and ruthenium in the same support (entry 7) results in an improvement in comparison to the test performed with each metal by its own, the metal amount used was reduced to the half and 62% conversion was obtained, with 50% and 15% selectivity towards **3** and **2** respectively, confirming that the synergy observed in batch reactions[17] is also present under a flow regime.

The reaction progress for the most promising catalyst, (Co_xO_y–N + RuO_x–N@C-irregular), is shown in Figure 2. Remarkably, the selectivity towards **2** increases with time. Within the timeframe of the experiment, a steady state in conversion (> 95% conversion of **1** after 100 min) was achieved, alas, with modest selectivity. Selectivity towards **3** is at its highest after 40 minutes (> 35%) and constantly decreases to 20% after 180 minutes. Similar behavior is observed for **4** and other by-products. Also, an unexpected product (**11**) (Figure 2 and scheme 4) was formed in relevant amounts (up to 20%).

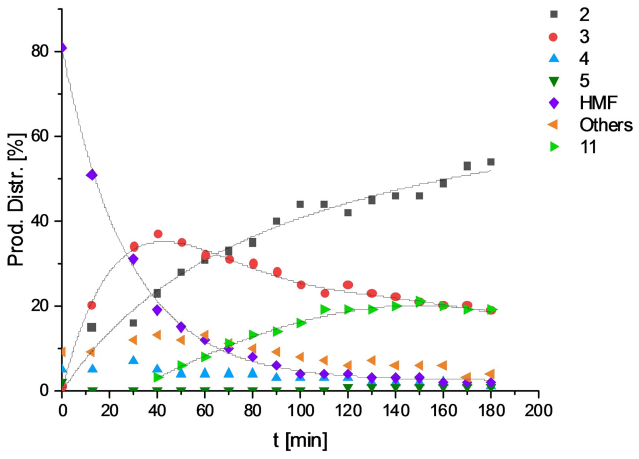

Figure 2. Reaction progress over time for the oxidative esterification of HMF using Co_xO_y–N + RuO_x–N@C-irregular as catalyst.

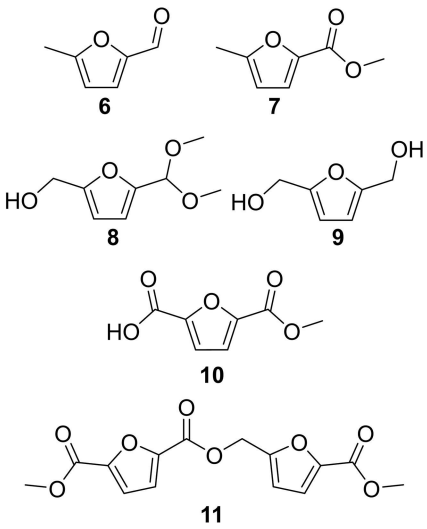

Scheme 4. By-products detected during the catalyst screening for the oxidative esterification of HMF under flow conditions.

As shown in table 1, side products could be detected in all experiments (labeled as "Others"). Those compounds that could be identified compounds are presented in Scheme 4.

5-methylfuran-2-carbaldehyde (**6**) is present in the starting solution of HMF, presumably as a decomposition product. From **6**, Methyl 5-methylfuran-2-carboxylate (**7**) would be obtained under the chosen reaction conditions. (5-(dimethoxymethyl) furan-2-yl)methanol (**8**) could be detected in the first samples collected in each experiment, indicating the acidic character of the catalysts at the first stages of the experiments, fostering the formation of acetals. Furan-2,5-diyldimethanol (**9**) is a side product arising from the eventual hydrogenation of **1** performed by the ruthenium catalysts. As we demonstrated before,[17] hydrogen gas was detected in the headspace of batch reactions, supporting this hypothesis. A mono-ester derivative of FDCA was detected, 5-(methoxycarbonyl)furan-2-carboxylic acid (**10**), which can arise from the partial hydrolysis of **2**. A compound with molecular mass and fragmentation patterns fitting to 2-((5-(methoxycarbonyl)furan-2-yl)methyl) 5-methyl furan-2,5-dicarboxylate (**11**) was also detected, suggesting that an esterification between **3** and **5** is possible under the reaction conditions.

As a general remark, the cobalt-containing catalysts having C-irregular as support are more active in the conversion of **1** (entries 5, 7 and 8) with a higher selectivity towards **2**. In the search for an explanation to this fact N_2 Physisorption analysis (BET measurements) were done on the raw supports and to the prepared catalysts (see Table 2).

The results show a marked difference in the surface area of each raw support (entries 1 and 6). C-pellets have more than twice the surface area of C-irregular, with 1178.3 m^2/g and 562.7 m^2/g, respectively. After the first impregnation and pyrolysis, the surface area is dramatically reduced: more than 40% for the C-pellets catalysts (entries 2 and 3), more than 75% for Co_xO_y–N@C-irregular (entry 7) and 60% for the RuO_x–N@C-

Table 2. N_2 Physisorption analysis for catalysts and supports.

Entry	Catalyst	Surface area [m^2/g]	Micropore area [m^2/g]	External surface area [m^2/g]
1	C-pellets	1178.3	1125.2	53.1
2	Co_xO_y–N@C-pellets	678.9	647.5	31.4
3	RuO_x–N@C-pellets	695.8	660.2	35.6
4	Co_xO_y–N + RuO_x–N@C-pellets	546.9	513.2	33.7
5	RuO_x–N + Co_xO_y–N@C-pellets	463.7	436.8	26.9
6	C-irregular	562.7	372.8	189.9
7	Co_xO_y–N@C-irregular	128.5	5.1	123.4
8	RuO_x–N@C-irregular	226.9	76.5	150.4
9	Co_xO_y–N + RuO_x–N@C-irregular	174.9	51.4	123.5
10	RuO_x–N + Co_xO_y–N@C-irregular	129.4	29.2	100.2

irregular catalyst (entry 8). The measurements after the second impregnation and pyrolysis show the same trend as in the case of the C-pellet catalysts (entries 4 and 5). Co_xO_y–N + RuO_x–N@C-pellets loses 19% of the starting surface area while RuO_x–N + Co_xO_y–N@C-pellets loses 33%. In contrast, the surface area of RuO_x–N + Co_xO_y–N@C-irregular is reduced by 43% (entry 10). Surprisingly, Co_xO_y–N + RuO_x–N@C-irregular (entry 9) presents an increase of almost 40% of the surface area compared to the starting material (Co_xO_y–N@C-irregular).

When the porosity of the materials (micropore area and external surface area) was studied, it can be observed that the C-pellet materials present a micropore:mesopore ratio of about 18:1 in comparison to 1:3 for the C-irregular ones. This is an important feature because in the conditions in which the experiments were performed porosity plays an important role in the diffusion of the substrate in the catalysts, which has a direct consequence on the conversion.[19] The better reactivity of C-irregular catalysts can be correlated with the abundance of mesopores in its structure in comparison to the C-pellet catalysts. The surface area provided by mesopores in the C-irregular materials is evidently higher, almost 4 times more than the C-pellets materials. Having a residence time of only 10 min, it is important that the substrate can easily diffuse into the catalysts' pores. It is know that micropores don't take part in the catalytic conversion of bulky molecules because the active sites within them cannot be reached by the substrates This renders them useless and therefore constitute a non-active surface in the catalysts.[20] For the residence time set in our experiments, the presence of mesopores is an important feature, as they are accessible to the bulky substrates and make the process less diffusion-limited.[21]

Additionally, XRD measurements of all the catalysts were done (See Supp. Info). Diffraction patterns of the all the samples supported on C-pellets show broad bands and low intensity peaks, which is evidence of a lack of crystallinity.[22] Conversely, the C-irregular catalysts show crystallinity. The Co_xO_y–N@C-irregular shows the same diffraction pattern as the Co_xO_y–N@C powder catalysts we previously used,[17,23] meaning that the particles in the new catalyst are similar to the powder analogue. Co_xO_y–N@C-irregular contains metallic cobalt, CoO and Co_3O_4. More interestingly, in the Co_xO_y–N + RuO_x–N@C-irregular catalyst it was possible to confirm the presence of metallic cobalt, but it was not possible to assign any refractions. Also, the diffraction pattern is not comparable with RuO_x–N + Co_xO_y–N@C-irregular. This shows that the order of addition of the metals has an influence in the type of catalyst obtained. The metal species present in both Co_xO_y–N + RuO_x–N@C-irregular and RuO_x–N + Co_xO_y–N@C-irregular are different.

In order gain a better understanding of the nature of the surface of the C-irregular catalysts, XPS characterization was performed. As expected, 3 different species of nitrogen were found. Pyridinic N-Metal, Pyrrolic N and Ammonia N (See Table 3).

The data in table 3 shows that we effectively produced nitrogen-doped catalysts and that the pyridinic nitrogen atoms bound to metal species is the more abundant type, an important fact that improves catalytic activity.[24]

Two ruthenium species are present at the surface, since not only Ru^0 but also $Ru^{4+}$was detected. All the samples contained mainly ~70% Ru^0 and ~30% Ru^{4+}. On the other side; using the Co 2p-peak shapes and the modified Auger parameter the existence of Co^{3+}in Co_xO_y–N@C-irregular, and both $Co^{2+}$and Co^{3+}in the bimetallic catalysts can be anticipated. Due to the low content of cobalt, its quantification was not possible due to the low signal-to-noise ratio.

A comparison between bulk elemental analysis and the elemental analysis of the surface measured by XPS, shows that the metallic species are located mostly at the surface of the material (see Table 4).

Since Co_xO_y–N@C-irregular is the starting material to synthesize Co_xO_y–N + RuO_x–N@C-irregular, the comparison between both elemental analyses (entries 1 and 3) allow us to see

Table 3. Nitrogen species detected by XPS.

Entry	Catalyst	Nitrogen species [%] Pyridinic N	Pyrrolic N	Ammon N
1	Co_xO_y–N@C-irregular	58	35	7
2	RuO_x–N@C-irregular	39	40	21
3	Co_xO_y–N + RuO_x–N@C-irregular	40	37	23
4	RuO_x–N + Co_xO_y–N@C-irregular	46	34	20

Table 4. Comparison of elemental analysis.

Entry	Catalyst	Location	Metal [wt%] Co	Ru
1	Co_xO_y–N@C-irregular	bulk	2.23	–
		surface	2.78	–
2	RuO_x–N@C-irregular	bulk	–	2.46
		surface	–	12.94
3	Co_xO_y–N + RuO_x–N@C-irregular	bulk	1.70	2.34
		surface	5.40	9.27
4	RuO_x–N + Co_xO_y–N@C-irregular	bulk	1.58	2.17
		surface	5.24	11.76

[a] Surface elemental analysis derived from identification of > 99,6% of atoms by XPS.

a migration process of the cobalt from the bulk to the surface of the material, most likely fostered by the incorporation of ruthenium. This result is supported by the increase in porosity observed for this catalyst: the mesoporous quantity remains similar but the micropore quantity increases in relation to the starting material. The migration of cobalt (Ostwald ripening) through the bulk creates new micropores.[25] A similar process was observed by Jones et al. in which, during pyrolysis of Co/Cu bimetallic catalysts, copper atoms migrate through the bulk to form Co-core Cu-shell particles increasing the amount of micropores in the material.[26]

This migration process is not observed for ruthenium in the synthesis of RuO_x–N + Co_xO_y–N@C-irregular. As can be seen in entries 2, 3 and 4, the ruthenium atoms remain mostly at the surface of the material. In comparison, the cobalt in Co_xO_y–N@C-irregular is distributed in a homogenous fashion. This difference is due to the temperature at which the pyrolysis is carried out; the Co atoms have enough energy to migrate in the bulk (i.e., lower Tamman temperature) but not the Ru ones.[27]

Performing the reaction under flow regime proved to be an improvement: in batch conditions full conversion to FDCM (**2**) is achieved in 18 h, representing a production of 0.03 mmol/h; in comparison, under flow conditions (Table 2 entry 6) in the last hour of the experiment >96% conversion of HMF (**1**) was obtained (1.44 mmol/h) and a selectivity to **2** of 44–54%, which represents a production of 0.47 mmol/h. Hence, the production of **2** under flow could be increased >15-fold compared to batch conditions.

Conclusions

The chemical modification of HMF is a challenge due to its inherent reactivity. Herewith, we report the oxidative esterification of HMF to FDCM under flow regime showing excellent conversion (98%) and good selectivity towards FDCM (57%). We were able to circumvent technical issues, by changing the catalyst support, identifying Co_xO_y–N + RuO_x–N@C-irregular as the best catalyst. The higher mesoporous surface related to the C-irregular catalysts is an important feature that provides improvement in conversion and selectivity.

Overall, under flow regime, a >15-fold increase on the production of FDCM was obtained in comparison to batch conditions. To the best of our knowledge this is the first report of oxidative esterification of HMF to FDCM under flow conditions. Further optimization of the process and studies to understand the nature of the supported catalysts is currently ongoing in our labs.

We hope that the findings in this paper provide a source of inspiration for the implementation of micro flow conditions in traditional organic transformations, but especially in the chemical modification of biomass-derived substrates.

Experimental Section

General experimental details

5-hydroxymethylfurfural (98%) was purchased from Fluorochem Ltd. and kept stored in a fridge. Methanol was purchased from Fischer Scientific and used as received. Oxygen (99. 99%) was purchased from Linde. $Co(OAc)_2 \cdot 4H2O$ was purchased from Abcr GmbH. Di-μ-chlorobi(p-cymene)chlororuthenium(II) (98%) was purchased from Acros Organics. 1,10-Phenanthroline was purchased from SIGMA-ALDRICH. The activated carbons, −20 + 40 mesh (Art. Nr. 45478) and 0.8 mm pellets (Art. Nr. L16334), were purchased from Alfa Aesar. The pyrolisis of the catalyst precursors was carried out in Centurion™ Neytech Qex Vacuum Furnace following the procedure previously reported by Beller et al.[28] ^1H and ^{13}C NMR spectra were recorded in $CDCl_3$ and with a Bruker Avance 300 with a QNP probe head (^1H: 300 MHz; ^{13}C: 75 MHz), or with a Bruker Avance 400 (^1H: 400 MHz; ^{13}C: 100 MHz). The calibration of the spectra was carried out using residual solvent shifts ($CDCl_3$, ^1H = 7.26, ^{13}C = 77.16) and were reported as parts per million relative to $SiMe_4$. All the NMR samples were measured at 24 °C. GC analysis was performed on a Hewlett-Packard 6890 Series chromatographer with MS and FID detectors. The elemental surface composition and chemical binding properties were analyzed by X-ray photoelectron spectroscopy (XPS) using an AXIS Ultra DLD electron spectrometer (Kratos Analytical, Manchester, UK). The spectra were recorded utilizing monochromatic X-rays Al kα (1486.6 eV) with a medium magnification (field of view 2) lens mode and with the slot mode selected. N_2 physisorption analyses were done with ASAP2010 instrument from Micromeritics (USA). The samples were pre-treated under Vacuum (0,001 mbar) at 400 °C for at least 3 h. Isotherms were recorded under standard BET conditions with adsorption of N_2 at −196 °C (cooling with liquid nitrogen). All calculations were done with ASAP2020 software V4.03 with standard parameters for BET, t-plot and BJH distribution. For micropore diameter and distribution the N_2-DFT model for slit pores with low regularisation was used. The SEM images of the carbon supports (C-pellets and C-irregular) were taken in a Carl Zeiss SUPRA 25 FESEM microscope operated by SmartSEM software.

Synthesis of the catalysts

RuOx–N@C-powder catalyst

$[Ru(p\text{-cymene})Cl_2]_2$ (154.6 mg, 0.26 mmol, corresponds to 5% Ru) and 1,10-Phenanthroline (83.0 mg, 0.46 mmol) were mixed in ethanol (50 mL) for 30 min. The carbon (759.3 mg) was added to the solution and heated to reflux at 100 °C for 4 hours. The solvent was evaporated and the resulting solid was thoroughly dried overnight at 60 °C under high vacuum. The black solid obtained was then pyrolyzed at 800 °C for 2 hours under argon atmosphere and cooled to room temperature. Elemental analysis (Wt%):C = 76.27, H = 0.332, N = 0.588, Ru = 5.51.

Co_xO_y + RuOx–N@C-powder catalyst

$Co(OAc)_2 \cdot 4H_2O$ (160,6 mg, mmol, corresponds to 3% wt Co) and $[Ru(p\text{-cymene})Cl_2]_2$ (154.6 mg, 0.26 mmol, corresponds to 5% wt Ru) were dissolved in 50 mL MeOH, after 5 min of vigorous stirring 1,10-phenanthroline (315.0 mg, mmol) was added. The solution was stirred for 30 min and carbon powder (412 mg) was added, then heated to reflux at 100 °C for 4 hours. The solvent was evaporated and the resulting solid thoroughly dried overnight at 60 °C under high vacuum. The black solid obtained was then pyrolyzed at 800 °C for 2 hours in argon atmosphere and cooled to room

temperature. Elemental analysis (Wt%): C = 70.08, H = 0.575, N = 1.633, Co = 4.83, Ru = 4.48.

Co_xO_y–N@C catalysts

$Co(OAc)_2 \cdot 4H_2O$ (380.4 mg, 1.53 mmol, corresponds to 3% wt Co) and 1,10-Phenanthroline (550.5 mg, 3.06 mmol) were mixed in ethanol (150 mL) for 30 min. The desired carbon (2069.1 mg) was added to the solution and heated to reflux at 100 °C for 4 hours. The solvent was evaporated and the resulting solid thoroughly dried overnight at 60 °C under high vacuum. The black solid obtained was then pyrolyzed at 800 °C for 2 hours in argon atmosphere and cooled to room temperature. −20 + 40 mesh particle size (C-irregular): Elemental analysis (Wt%):C = 72.75, H = 0.477, N = 1.745, Co = 2.23. XPS data (atom %): C = 90.1, O = 5.9; N = 2.1, Si = 0.8; S = 0.2; Co = 0.6. 0,8 mm pellets (C-pellets): Elemental analysis (Wt%): C = 85,40, H = 0,3954, N = 3,961, Co = 2,34.

RuO_x–N@C catalysts

$[Ru(p\text{-cymene})Cl_2]_2$ (463.8 mg, 0.74 mmol, corresponds to 5% wt Ru) and 1,10-Phenanthroline (266.7 mg, 1.48 mmol) were mixed in ethanol (150 mL) for 30 min. The desired carbon (2269.5 mg) was added to the solution and heated to reflux at 100 °C for 4 hours. The solvent was evaporated and the resulting solid thoroughly dried overnight at 60 °C under high vacuum. The black solid obtained was then pyrolyzed at 800 °C for 2 hours in argon atmosphere and cooled to room temperature. −20 + 40 mesh particle size(C-irregular): Elemental analysis (Wt%): C = 65.40, H = 0.4507, N = 1.167, Ru = 2.46. XPS data (atom %): C = 89.2, O = 6.9, N = 0.9, Si = 0.7, S = 0.3; Ru = 1.8. 0,8 mm pellets (C-pellets): Elemental analysis analysis (Wt%): C = 83.12, H = 0.4507, N = 0.850, Ru = 1.79.

Bimetallic Co_xO_y–N + RuO_x–N@C catalysts

$[Ru(p\text{-cymene})Cl_2]_2$ (231.9 mg, 0.38 mmol, corresponds to 5% wt Ru) and 1,10-Phenanthroline (133.3 mg, 0.74 mmol) were mixed in ethanol (75 mL) for 30 min. The previously prepared Co_xO_y–N@C catalyst (1143.8 mg) was added to the solution and heated to reflux at 100 °C for 4 hours. The solvent was evaporated and the resulting solid thoroughly dried overnight at 60 °C under high vacuum. The black solid obtained was then pyrolyzed at 800 °C for 2 hours in argon atmosphere and cooled to room temperature. −20 + 40 mesh particle size (C-irregular): Elemental analysis (Wt%): C = 68.86, H = 0.5722, N = 1.746, Co = 1.70, Ru = 2.34. XPS data (atom %): C = 88.3, O = 6.9, N = 1.3, Si = 0.5, S = 0.2, Co = 1.3, Ru = 1.3. 0,8 mm pellets (C-pellets): Elemental analysis (Wt%): C = 72.35, H = 0.1247, N = 1.789, Co = 1.48, Ru = 0.56

Bimetallic RuO_x–N + Co_xO_y–N@C catalysts

$Co(OAc)_2 \cdot 4H_2O$ (190.2 mg, 0.765 mmol, corresponds to 3% wt Co) and 1,10-Phenanthroline (275.3 mg, 1.53 mmol) were mixed in ethanol (75 mL) for 30 min. The previously prepared RuO_x–N@C catalyst (1034.5 mg) was added to the solution and heated to reflux at 100 °C for 4 hours. The solvent was evaporated and the resulting solid thoroughly dried overnight at 60 °C under high vacuum. The black solid obtained was then pyrolyzed at 800 °C for 2 hours in argon atmosphere and cooled to room temperature. −20 + 40 mesh particle size (C-irregular): Elemental analysis (Wt%): C = 85.33, H = 0.6427, N = 3.007, Co = 1.58, Ru = 2.17. XPS data (atom %): C = 86.0, O = 7.7, N = 1.9, Si = 0.6, S = 0.4, Co = 1.3; Ru = 1.7. 0,8 mm pellets (C-pellets): Elemental analysis (Wt%): C = 54.11, H = 0.0802, N = 1.770, Co = 1.26, Ru = 1.20.

Flow microreactor setup

All the reactions were carried out using the Modular MicroReaction System (MMRS) from Ehrfeld Mikrotechnik. The solution was pumped with a HPLC-pump (Knauer). The oxygen flow was controlled with an EL-FLOW Mass Flow Controller from Bronkhorst, for the gas/liquid mixing a multilamination mixer was used. The catalyst was applied in a cartridge Reactor F200 with temperature indicator. The total volume of the setup was ~7–8 mL.

Oxidative esterification of HMF

A desired amount of K_2CO_3 was let to dissolve in MeOH overnight at room temperature under vigorous stirring, once the K_2CO_3 was completely dissolved HMF was added, additional MeOH was added until a solution with the concentration of 0.125 M in HMF and 0.025 M in K_2CO_3 was reached. 600 mg of catalyst was loaded into the cartridge of the reactor before the heating and a flow of MeOH and oxygen were started. Once the temperature, pressure and flows (liquid and gas) in the system were stable (after ~45–60 min) the HMF/K_2CO_3 solution was pumped through and the reaction was started. The solution coming at the end of the setup was collected and analyzed by gas chromatography.

Isolation of compounds

An automated flash chromatography system with UV detection was used (CombiFlashRf from Teledyne ISCO), using a silica column and heptane/ethyl acetate as solvents. The solvent flow was set up to 30 mL/min. The solvent setup was configured as follows, from start to min 20 the concentration increased from 0% to 45% ethyl acetate; the mixture was kept to min 32, and from min 32 to min 42 the concentration increased from 45% to 100% ethyl acetate; which was kept flowing until the column was completely washed. The compounds obtained were analyzed by NMR and GC-MS.

Acknowledgements

This work has been supported by the Leibniz Society (Project: Agro and paper industry waste to bulk chemicals. Levulinic acid and furfural as platform chemicals) and by the RoHan Project funded by the German Academic Exchange Service > (DAAD, No. 57315854) and the Federal Ministry for Economic Cooperation and Development (BMZ) inside the framework "SDG Bilateral Graduate school programme". For the microreactor setup financial support from "Fonds der Chemischen Industrie" is gratefully acknowledged. Special thanks to Khathiravan Murugesan for his assistance in the preparation of the catalysts.

Conflict of Interest

The authors declare no conflict of interest.

Keywords: 5-hydroxymethylfurfural · Oxidation · Heterogeneous catalysis · dimethyl-2,5-furandicarboxylate · Flow chemistry · Microreactor

[1] J. H. Clark, T. J. Farmer, L. Herrero-Davila, J. Sherwood, *Green Chem.* **2016**, *18*, 3914–3934.
[2] J. G. de Vries, *Chem. Rec.* **2016**, *16*, 2783–2796.
[3] A. F. Sousa, C. Vilela, A. C. Fonseca, M. Matos, C. S. R. Freire, G.-J. M. Gruter, J. F. J. Coelho, A. J. D. Silvestre, *Polym. Chem.* **2015**, *6*, 5961–5983.
[4] a) S. K. Burgess, J. E. Leisen, B. E. Kraftschik, C. R. Mubarak, R. M. Kriegel, W. J. Koros, *Macromolecules* **2014**, *47*, 1383–1391; b) E. F. Efsa Panel on Food Contact Materials, A. Processing, *EFSA Journal* **2014**, *12*, 3866–3874; c) A. Pellis, K. Haernvall, C. M. Pichler, G. Ghazaryan, R. Breinbauer, G. M. Guebitz, *J. Biotechnol.* **2016**, *235*, 47–53.
[5] F. Lin, K. Wang, L. Gao, X. Guo, *Appl. Organomet. Chem.* **2019**, *33*, e4821.
[6] R. Fromanger, S. E. Guillouet, J. L. Uribelarrea, C. Molina-Jouve, X. Cameleyre, *J. Ind. Microbiol. Biotechnol.* **2010**, *37*, 437–445.
[7] A. Mohsenzadeh, A. Zamani, M. J. Taherzadeh, *ChemBioEng Rev.* **2017**, *4*, 75–91.
[8] M. G. Gert-Jan, S. Laszlo, D. Matheus Adrianus, *Comb. Chem. High Throughput Screening* **2012**, *15*, 180–188.
[9] a) L. Gao, W. Zhuge, X. Feng, W. Sun, X. Sun, G. Zheng, *New J. Chem.* **2019**, *43*, 8189–8194; b) I. Graca, S. Al-Shihri, D. Chadwick, *Appl. Catal. A* **2018**, *568*, 95–104.
[10] a) R. Battino, T. R. Rettich, T. Tominaga, *J. Phys. Chem. Ref. Data* **1983**, *12*, 163–178; b) P. M. Osterberg, J. K. Niemeier, C. J. Welch, J. M. Hawkins, J. R. Martinelli, T. E. Johnson, T. W. Root, S. S. Stahl, *Org. Process Res. Dev.* **2015**, *19*, 1537–1543.
[11] a) D. Dallinger, C. O. Kappe, *Curr. Opin. Green Sustainable Chem.* **2017**, *7*, 6–12; b) B. Gutmann, D. Cantillo, C. O. Kappe, *Angew. Chem. Int. Ed.* **2015**, *54*, 6688–6728; *Angew. Chem.* **2015**, *127*, 6788–6832; c) N. Kockmann, P. Thenée, C. Fleischer-Trebes, G. Laudadio, T. Noël, *React. Chem. Eng.* **2017**, *2*, 258–280.
[12] a) M. B. Plutschack, B. Pieber, K. Gilmore, P. H. Seeberger, *Chem. Rev.* **2017**, *117*, 11796–11893; b) H. P. L. Gemoets, Y. Su, M. Shang, V. Hessel, R. Luque, T. Noël, *Chem. Soc. Rev.* **2016**, *45*, 83–117.
[13] M. Gruenewald, J. Heck, *Chem. Ing. Tech.* **2015**, *87*, 1185–1193.
[14] C. A. Hone, C. O. Kappe, *Top. Curr. Chem.* **2018**, *377*, 2.
[15] V. Hessel, P. Löb, H. Löwe, in *Microreactors in Organic Synthesis and Catalysis* (Ed.: T. Wirth), Wiley, **2008**, pp. 211–275.
[16] M. Sajid, X. Zhao, D. Liu, *Green Chem.* **2018**.
[17] A. Salazar, P. Hünemörder, J. Rabeah, A. Quade, R. V. Jagadeesh, E. Mejia, *ACS Sustainable Chem. Eng.* **2019**, DOI: 10.1021/acssuschemeng.1029b00914.
[18] P. Kluson, L. Cerveny, J. Had, *Catal. Lett.* **1994**, *23*, 299–212.
[19] R. A. v. Santen, in *Modern Heterogeneous Catalysis*, **2017**, pp. 59–116.
[20] C. Perego, A. Carati, P. Ingallina, M. A. Mantegazza, G. Bellussi, *Appl. Catal. A* **2001**, *221*, 63–72.
[21] C. Perego, R. Millini, *Chem. Soc. Rev.* **2013**, *42*, 3956–3976.
[22] B. D. Cullity, S. R. Stock, *Elements of X-Ray Diffraction*, 3rd ed., Pearson, **2013**.
[23] R. V. Jagadeesh, H. Junge, M.-M. Pohl, J. Radnik, A. Brückner, M. Beller, *J. Am. Chem. Soc.* **2013**, *135*, 10776–10782.
[24] D. Formenti, F. Ferretti, C. Topf, A.-E. Surkus, M.-M. Pohl, J. Radnik, M. Schneider, K. Junge, M. Beller, F. Ragaini, *J. Catal.* **2017**, *351*, 79–89.
[25] a) T. W. Hansen, A. T. DeLaRiva, S. R. Challa, A. K. Datye, *Acc. Chem. Res.* **2013**, *46*, 1720–1730; b) P. J. F. Harris, *Int. Mater. Rev.* **1995**, *40*, 97–115.
[26] K. W. Golub, T. P. Sulmonetti, L. A. Darunte, M. S. Shealy, C. W. Jones, *ACS Appl. Nano Mater.* **2019**.
[27] a) J. A. Moulijn, A. E. van Diepen, F. Kapteijn, *Appl. Catal. A* **2001**, *212*, 3–16; b) M. D. Argyle, C. H. Bartholomew, *Catalysts* **2015**, *5*, 145–269.
[28] R. V. Jagadeesh, T. Stemmler, A.-E. Surkus, M. Bauer, M.-M. Pohl, J. Radnik, K. Junge, H. Junge, A. Bruckner, M. Beller, *Nat. Protoc.* **2015**, *10*, 916–926.

Manuscript received: February 6, 2020
Revised manuscript received: April 13, 2020
Accepted manuscript online: April 15, 2020
Version of record online: May 12, 2020